Dynamic entity formed by protein and its hydration water

Yongfeng Ye,[1,2,*] Xiaoxia Chen,[2,*] Juan Huang,[3] Lirong Zheng,[1,2] Qingxue Tang,[4] Liuliu Long,[5] Takeshi Yamada,[6] Madhusudan Tyagi,[7] Victoria García Sakai,[8] Hugh O'Neill,[9] Qiu Zhang,[9] Nicolas R. de Souza,[10] Xiang Xiao,[4,11,12] Weishu Zhao,[4,11,12,†] Liang Hong,[1,2,13,14,15,‡] and Zhuo Liu[2,13,14,15,§]

[1]*School of Physics and Astronomy, Shanghai Jiao Tong University, Shanghai 200240, China*
[2]*Institute of Natural Sciences, Shanghai Jiao Tong University, Shanghai 200240, China*
[3]*School of Chemistry and Chemical Engineering, Shanghai Jiao Tong University, 800 Dongchuan Road, Shanghai 200240, China*
[4]*State Key Laboratory of Microbial Metabolism, School of Life Sciences and Biotechnology, Shanghai Jiao Tong University, Shanghai 200240, China*
[5]*School of Physical Science and Technology, ShanghaiTech University, Shanghai 201210, China*
[6]*Neutron Science and Technology Center, Comprehensive Research Organization for Science and Society, 162-1 Shirakata, Tokai, Naka, Ibaraki 319-1106, Japan*
[7]*National Institute of Standards and Technology (NIST), NIST Center for Neutron Research, Gaithersburg, Maryland 20899, USA and Department of Materials Science and Engineering, University of Maryland, College Park, Maryland 20742, USA*
[8]*ISIS Pulsed Neutron and Muon Source, Rutherford Appleton Laboratory, Science & Technology Facilities Council, Didcot OX11 0QX, United Kingdom*
[9]*Biology and Soft Matter Division, Oak Ridge National Laboratory, Oak Ridge, Tennessee 37931, USA*
[10]*Australian Nuclear Science and Technology (ANSTO), Locked Bag 2001, Kirrawee DC, NSW 2232, Australia*
[11]*International Center for Deep Life Investigation, Shanghai Jiao Tong University, Shanghai 200240, China*
[12]*SJTU Yazhou Bay Institute of Deepsea Sci-Tech, Yongyou Industrial Park, Sanya 572024, China*
[13]*Shanghai National Centre for Applied Mathematics (SJTU Center), MOE-LSC, Shanghai Jiao Tong University, Shanghai 200240, China*
[14]*Zhangjiang Institute for Advanced Study, Shanghai Jiao Tong University, Shanghai 201203, China*
[15]*Shanghai Artificial Intelligence Laboratory, Shanghai 200232, China*

(Received 29 April 2024; accepted 1 September 2024; published 19 September 2024)

The interaction between protein and water plays a pivotal role in shaping the structure, dynamics, and function of biomacromolecules. A comprehensive understanding of this intricate interplay necessitates a systematic evaluation of interaction strength and its consequential impact on the dynamics of proteins and water across diverse protein systems. Despite numerous works on understanding the dynamics of water and proteins and the coupling between them, there are still unanswered questions. Here, we combine neutron scattering and isotope labeling to probe the dynamics of proteins and their hydration water in a variety of protein systems. We consider proteins of different structures and varying thermostability as well as proteins within living cells with distinct growth temperatures. Simultaneous characterization of protein and hydration water dynamics across diverse systems was achieved. Moreover, we performed water sorption isothermal measurements on three representative proteins to correlate the observed dynamics with the strength of the interaction energies governing each system. The experimental results underscore that proteins manifesting stronger attractive interactions with water display diffusionlike dynamics with higher flexibility upon hydration, concomitant with a reduced mobility in hydration water. Significantly, our findings suggest that, in fact, it is the interaction between protein and its hydration water that facilitates the transfer of mobility from water to protein, with stronger interactions correlating to greater protein flexibility and slower hydration water diffusion.

DOI: 10.1103/PhysRevResearch.6.033316

I. INTRODUCTION

Protein hydration water assumes pivotal roles in numerous biological activities, encompassing but not limited to protein folding, ligand recognition, proton transfer, and enzymatic catalysis [1–3]. A comprehensive exploration of these diverse functions necessitates a meticulous examination of the dynamics of both protein and its hydration water, coupled with an in-depth understanding of their intricate interactions. To probe these dynamics, researchers have employed a diverse array of experimental techniques, such as nuclear magnetic resonance (NMR) [4–6], neutron scattering

*These authors contributed equally to this work.
†Contact author: zwsh88@sjtu.edu.cn
‡Contact author: hongl3liang@sjtu.edu.cn
§Contact author: judeliu@sjtu.edu.cn

[7–11], femtosecond fluorescence spectroscopy [12–14], and dielectric spectroscopy [15–17], among others [18–21]. Complementary insights into molecular details of protein-water interactions have been gleaned through the application of molecular dynamics (MD) simulations [22–25]. The discussion on protein-water interaction has seen an abundance of research, with only a fraction of the literature cited. Despite these endeavors, the intricate interplay between protein and its hydration water remains a subject of extensive debate. Notably, Frauenfelder *et al.* [15,26] and Fenimore *et al.* [16] have posited a coupling effect between conformational fluctuations in proteins and the dynamics of the solvent, primarily composed of water molecules. However, insights drawn from NMR [27] and electron spin resonance [28] studies suggest a potential decoupling of the dynamics of internal protein residues from that of the solvent. Furthermore, predominant studies on the hydration water of intrinsically disordered proteins (IDPs) consistently reveal more restricted water motions on the IDP surface than folded proteins [7,29–32]. Conversely, a simulation study has suggested that water molecules hydrating a disordered protein ($A\beta_{1-42}$) exhibit relatively faster dynamics than those hydrating a globular protein (ubiquitin) [33]. Consequently, a more profound understanding of protein-water interactions demands the simultaneous characterization of the individual dynamics of protein and its hydration water across a spectrum of protein-water model systems.

Neutron scattering is an ideal technique to probe dynamics in biological systems, as one can probe water and biomass independently. Moreover, it has also been proven to be useful to look not only at model systems but at real, more complex, systems, e.g., living cells [34]. The versatility of neutron instruments, with varying energy resolutions, provides a valuable means to explore the dynamics of the proteome [35,36], hydration water [37,38], and bulklike water [39,40] within living cells. Notably, neutron instruments with energy resolutions of 0.8 and 17 μeV can probe the motions at the time scales of ∼1 ns and ∼60 ps and thereby have been used to elucidate the diffusionlike dynamics of the proteome and intracellular water in *Escherichia coli*, respectively [36,39]. The substantial incoherent scattering cross-section of hydrogen (H), exceeding that of other elements by at least an order of magnitude, bestows upon neutron scattering the distinctive ability to discern the diffusion dynamics of hydration water from those of the protein, and vice versa, particularly through isotopic labeling. This inherent capability establishes neutron scattering as an ideal methodology for characterizing the individual dynamics of protein and its hydration water within a hydrated protein system [24,29,41]. In addition to probing the diffusion dynamics of protein and its hydration water, neutron and x-ray scattering can characterize a range of complex protein collective dynamics involving the so called *fast sound* in the terahertz range, extending beyond the diffusionlike motions discussed above. For instance, Brillouin-like low-frequency collective modes have been observed in both dry and hydrated proteins by means of neutron scattering [42,43]. The structural and dynamical properties of hydrated proteins, as measured by x-ray scattering, have been demonstrated to correlate with the short-time collective vibrational motions intrinsic to proteins [44]. Additionally, collective dynamics are also observed in water [45–49] and other biochemical systems, such as DNA [50,51], lipid membranes [52,53], and living cells [54] using coherent neutron scattering. Importantly, both diffusionlike dynamics and fast collective vibrational motions of protein and its hydration water can affect the functionality of the biological molecules.

In this paper, neutron instruments with variable resolutions were employed to assess the diffusionlike dynamics of the proteome and its hydration water in diverse living cells. The proteome of the mesophile displayed the highest flexibility, followed by the thermophile, while the hyperthermophile showed the most rigid proteome dynamics. Conversely, the hydration water of the mesophile exhibited the slowest movement, contrasting with the hydration water of the hyperthermophile, which demonstrated the most rapid diffusion. Additionally, three groups of globular proteins with distinct structures were selected for a more detailed investigation. Combining neutron scattering with isotope labeling, we probed the diffusionlike dynamics of individual proteins within each group and their corresponding hydration water dynamics. Strikingly, an inverse correlation was observed between the dynamics of a hydrated protein and its hydration water, indicating that protein with greater flexibility exhibited slower motion of its hydration water across all three protein groups. This observation aligns with prior reports emphasizing the increased flexibility of IDPs compared with globular, folded proteins, along with more restricted water motions on the IDP surface [29]. Moreover, water sorption isothermal experiments suggested that proteins with stronger attractive interactions with water displayed increased flexibility upon hydration. These experimental findings unveil the potential scenario wherein protein may acquire mobility from its hydration water through interaction, highlighting the formation of a dynamic entity through the coupling between protein and water.

II. MATERIALS AND METHODS

A. Materials

All cellular specimens and cytochrome P450s (CYPs) underwent preparation at Shanghai Jiao Tong University (SJTU). The provision of green fluorescence protein (GFP) was facilitated by H.O. and Q.Z. at Oak Ridge National Lab. Hydrogenated lysozyme (LYS) sourced from chicken egg white, hydrogenated myoglobin (MYO) from equine skeletal muscle, and deuterium oxide (D_2O, 99.9 atom % D) were procured from Sigma Aldrich (Shanghai, China).

B. Sample preparation

E. coli BL21 underwent aerobic cultivation in LB medium at 37 °C, whereas *Zhurongbacter thermophilus* 3DAC and *Thermococcus eurythermalis* A501 were anaerobically cultured in TRM medium which contained 4 g/L tryptone, 1 g/L yeast extract, 23 g/L NaCl, 5 g/L $MgCl_2 \bullet 6H_2O$, 0.02 g/L $CaCl_2$, 0.01 g/L $SrCl_2$, 0.05 g/L NaBr, 1 mL 10 mM $NaWO_4$, 0.06 g/L KH_2PO_4, 0.06 g/L K_2HPO_4, 0.5 mL/L Resazurin, and 1 mL 25 mM $FeCl_3 \bullet 6H_2O$ (pH 7.0 and 2.3% NaCl) at 70 and 85 °C, respectively, following previously established batch culture procedures [36,55,56]. Harvesting of all cells occurred during the late exponential phase through centrifugation at 6000 × *g* at 4 °C for 10 min. Subsequently, the cell

samples were converted into aluminum sample containers for neutron scattering in anaerobic conditions and stored within anaerobic bags.

Prior to usage, LYS and MYO underwent dialysis. Cytochrome P450 101 (CYP101), cytochrome P450 119 (CYP119), and GFP were internally prepared in both hydrogenated and perdeuterated forms. The expression and purification protocols for hydrogenated and perdeuterated CYP101, CYP119, and GFP adhered to previously outlined methods [57–59]. For simplicity, the prefixes H and D denote hydrogenated and perdeuterated, respectively. All five hydrogenated proteins were dissolved in D_2O to ensure the exchangeable hydrogen atoms underwent deuteration, followed by a 12 h lyophilization period. Similarly, the exchangeable deuterium atoms in D-CYP and D-GFP were replaced with hydrogens by dissolving them in H_2O, subsequently undergoing lyophilization.

The protein hydration process was executed within a glove box, partially filled with H_2O (or D_2O), and subjected to inert gas purging to mitigate atmospheric water interference [60]. Protein samples were hermetically sealed in a desiccator to facilitate water adsorption until achieving the desired hydration level (h, gram water/gram protein). The determination of hydration levels relied on precise weight measurements before and after water adsorption. Ultrapure water (H_2O) was sourced from a Millipore Direct-Q system (18.2 MΩ cm at 25 °C), while deuterium oxide (D_2O, 99.9 at. % D) was procured from Sigma Aldrich (Shanghai, China). The resulting samples for elastic and quasielastic neutron scattering (QENS) are detailed in Table S1 in the Supplemental Material [61], with the protein samples meticulously sealed in aluminum cans within the glove box before neutron scattering experiments.

C. Determination of the chemical compositions of 3DAC and A501

DNA, RNA, and proteins were concurrently isolated utilizing a coextraction methodology to elucidate the chemical compositions of 3DAC and A501. Differential solubilities in organic and inorganic solutions facilitated the simultaneous separation of nucleic acids and proteins from a singular sample. Subsequent extraction involved the individual isolation of nucleotides, with $\frac{1}{3}$ allocated for DNA purification and the remaining $\frac{2}{3}$ for RNA purification, while all proteins underwent purification. Concentrations of DNA, RNA, and protein (expressed in mg/mL) were assessed using nanodrop. The concrete volume of the solution was precisely determined through the DNA and RNA dissolution process during coextraction. The quantification of the weight of isolated DNA, RNA, and protein was conducted by considering the specific volume and concentration of their respective solutions. The total weights of DNA and RNA were adjusted based on a factor of 3 and $\frac{3}{2}$ according to the ration of volume utilization of nucleotides solution. The resulting relative dry weights are detailed in Table S2 in the Supplemental Material [61].

D. Small angle x-ray scattering (SAXS)

In situ synchrotron small angle x-ray scattering (SAXS) measurements were performed at the BL19U2 beamline within the Shanghai Synchrotron Radiation Facility (SSRF), utilizing an x-ray wavelength of 0.103 nm. *E. coli* samples were dissolved in LB medium, while 3DAC and A501 were dissolved in TRM medium supplemented with 1% (v/v) Na_2S to prohibit the influence of oxygen. Each strain maintained a cell density of $\sim 0.7 \times 10^8$ mL^{-1}. For uniform suspension, samples were carefully resuspended with a pipet before measurements. The cell suspensions were loaded into a silica cell and gently refreshed using a syringe pump to prevent x-ray damage. Measurements were conducted at various temperatures ranging from 25 to 70 °C, with a heating rate of 5 °C/ min, and each sample was equilibrated for 10 min at each measuring temperature. To calculate the absolute intensity of the samples, empty cells and buffers were measured at corresponding temperatures. Two-dimensional (2D) diffraction patterns were captured by the Pilatus 2 M detector, featuring a resolution of 1043 × 981 pixels with dimensions of 172 × 172 μm. Twenty consecutive 2D images were acquired, each with a 1 s exposure time per frame. These 2D scattering patterns were subsequently integrated into one-dimensional (1D) intensity curves using the RAW software [62], with frames exhibiting no radiation damage selected for further processing.

E. QENS

The QENS signal manifests as a broadening around the elastic line and is ascribed to diverse motions occurring within the temporal constraints of the spectrometer. In the context of a neutron scattering experiment, insights into MD are gleaned by evaluating the dynamic structure factor, denoted as $S(\mathbf{q}, \Delta E)$. This factor encapsulates the likelihood of an incident neutron partaking in a scattering event, involving the transfer of both momentum ($\mathbf{q}$) and energy (ΔE). The resultant experimental scattering function $S_{\text{measured}}(\mathbf{q}, \Delta E)$ can be represented by

$$S_{\text{measured}}(\mathbf{q}, \Delta E) = \exp\left(-\frac{\hbar\omega}{2k_B T}\right) R(\mathbf{q}, \Delta E) \otimes S(\mathbf{q}, \Delta E), \tag{1}$$

where $\exp(-\hbar\omega/2k_B T)$ is a detailed balance factor, and $R(\mathbf{q}, \Delta E)$ denotes the experimentally determined resolution function, convoluted with the scattering model $S(\mathbf{q}, \Delta E)$. This model encapsulates the dynamic intricacies of the sample, comprehensively addressing all components of its dynamical system. In hydrogenous samples, the dominance of incoherent scattering in $S(\mathbf{q}, \Delta E)$ is noteworthy, given the substantially higher incoherent scattering cross-section of hydrogen atoms than other atoms. The term $S_{\text{inc}}(\mathbf{q}, \Delta E)$ corresponds to the self-correlation function or incoherent dynamic structure factor, expressed as the summation of both elastic and inelastic contributions:

$$\begin{aligned} S_{\text{inc}}(\mathbf{q}, \Delta E) = {} & \exp(-\mathbf{q}^2\langle u^2\rangle) A_0(\mathbf{q})\delta(\Delta E) \\ & + [1 - A_0(\mathbf{q})] L(\mathbf{q}, \Delta E), \end{aligned} \tag{2}$$

where the exponential term, $\exp(-\boldsymbol{q}^2\langle u^2\rangle)$, is the Debye-Waller factor, $A_0(\mathbf{q})\delta(\Delta E)$ delineates the elastic contribution attributed to motions exhibiting time scales slower than the longest observable time, dictated by the energy resolution of

the spectrometer. The subsequent term in the equation characterizes the quasielastic component. The direct provision of temporal and spatial information on the investigated system is facilitated by $S_{\rm inc}(\mathbf{q}, \Delta E)$ directly provides time/space information on the system investigated: temporal insights are derived from the neutron energy transfer (ΔE), and spatial characteristics are elucidated through the momentum scattering transfer ($\mathbf{q}$). As the QENS data in the time domain are inherently exponential, their representation in the energy domain involves the approximation using Lorentzian functions with varying widths, Γ [full width at half maximum (FWHM) = 2 × half width at half maximum (HWHM)], describing motions transpiring on diverse time scales:

$$L(x) = \frac{1}{\pi}\frac{\Gamma}{\Gamma^2 + \left(\frac{\Delta E}{\hbar}\right)^2}. \tag{3}$$

The examination of the dependency of each Γ value on $\mathbf{q}$ enables a comprehensive analysis, offering detailed insights into the distinct dynamical components that collectively contribute to the comprehensive QENS profile observed in the experimental setup.

FWHM parameters were derived from the Lorentzian functions characterizing specific dynamical components inherent in the system. This extraction facilitated the determination of key parameters such as translational diffusion coefficients ($D_{\rm T}$), jump times ($\tau_{\rm T}$), and correlation times associated with localized motions of cellular macromolecules ($\tau_{\rm L}$). The analysis of translational Lorentzians incorporated a jump-reorientation mechanism, described by the equation [63,64]:

$$\Gamma_{\rm T}(\mathbf{q}) = \frac{D_{\rm T}\mathbf{q}^2}{1 + D_{\rm T}\mathbf{q}^2\tau_{\rm T}^{\rm jump}}, \tag{4}$$

where $D_{\rm T}$ denotes the translational coefficient at temperature T, while $\tau_{\rm T}^{\rm jump}$ corresponds to the translational jump time, signifying the mean residence time of a water molecule within each conceivable location.

The QENS data for *E. coli*, 3DAC, and A501 cell samples were acquired using the DNA spectrometer at J-PARC in Japan, employing a resolution of 13 μeV. The experiments covered a $\mathbf{q}$ range from 0.025 to 1.975 Å^{-1} and an energy transfer window from −500 to 1500 μeV. The data collection for *E. coli*, 3DAC, and A501 occurred in the temperature ranges of 4–30, 4–70, and 4−70 °C, respectively, employing a heating rate of 1.0 K/min. Corrections for detector efficiency were applied to the QENS spectra, and resolution functions were independently determined through calibration runs for vanadium. The QENS spectra fitting, performed within the $\mathbf{q}$ range of 0.325–1.825 Å^{-1} and energy transfer range of −500 to 1500 μeV, utilized the MANTID program 6.8.0 [65]. The fitting incorporated one delta function (representing the elastic component) and three Lorentzians (representing quasielastic contributions), as illustrated in Fig. S1 in the Supplemental Material [61] (see also Refs. [29,66–70] therein). These components were assigned to specific dynamical populations: (1) very slow motions of the largest organelles, cytoskeleton, and global macromolecular motions within the cell; (2) slow diffusion of cellular water molecules (hydration water); (3) fast diffusion of cellular water molecules (bulklike water); and (4) internal localized motions of macromolecules and/or fast rotation of water molecules within the cellular medium. The extraction of dynamic information regarding hydration water in the cell was achieved through the fitting of the QENS curves (Fig. S2 in the Supplemental Material [61]).

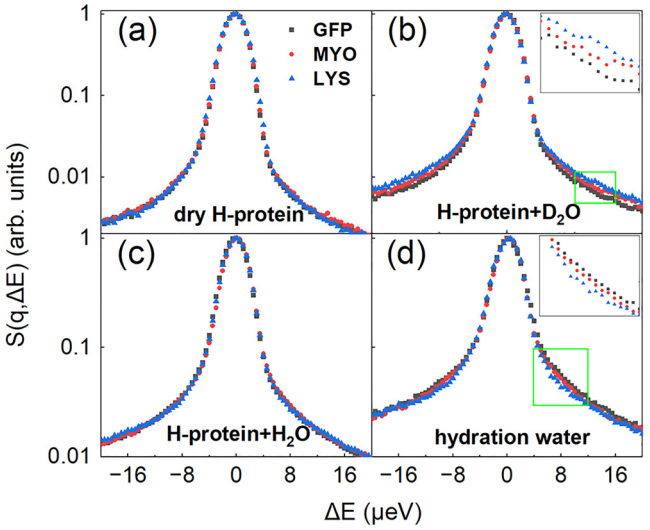

FIG. 1. Dynamics of three representative globular proteins and their hydration water. (a) Dynamic structure factor $S(\mathbf{q}, \Delta E)$ of lyophilized hydrogenated green fluorescence protein (GFP), myoglobin (MYO), and lysozyme (LYS), which are denoted as "dry H-protein." $S(\mathbf{q}, \Delta E)$ of hydrogenated GFP, MYO, and LYS hydrated in (b) D_2O and (c) H_2O at $h = 0.3$, which are denoted as "H-protein + D_2O" and "H-protein + H_2O," respectively. (d) $S(\mathbf{q}, \Delta E)$ of hydration water, obtained as the difference between $S(\mathbf{q}, \Delta E)$ of H-protein + H_2O and that of H-protein + D_2O, denoted as "hydration water." GFP, MYO, and LYS are represented by black squares, red dots, and blue triangles, respectively. The insets in (b) and (d) illustrate the local details of the spectra for H-protein + D_2O and hydration water, which are enclosed in green blocks. Spectra were collected at DNA with a resolution of 3 μeV at 280 K and normalized to maximum peak intensity.

For CYP101 and CYP119, the QENS spectra were obtained in D-protein + H_2O form at 280 K using the OSIRIS instrument with a resolution of 25.4 μeV at ISIS in the UK. The experimental data covered a $\mathbf{q}$ range from 0.244 to 1.814 Å^{-1}, capturing the energy transfer window from −376 to 1420 μeV.

For the three representative globular proteins, namely, GFP, LYS, and MYO, QENS were conducted on dry H-protein, H-protein + D_2O, and H-protein + H_2O form at 280 K. The experiments were carried out using the DNA spectrometer with a resolution of 3 μeV and within the energy transfer range from −40 to 100 μeV at J-PARC in Japan. The acquired $S(\mathbf{q}, \Delta E)$ data were integrated over the $\mathbf{q}$ range spanning from 0.175 to 1.825 Å^{-1} and normalized to ensure consistent peak intensities over energy for comparative analysis. To elucidate the $S(\mathbf{q}, \Delta E)$ of hydration water on H-proteins [see Fig. 1(d)], we performed spectral subtraction by appropriately normalizing the spectra of H-protein + D_2O and H-protein + H_2O, ensuring the ratio of integrals of their corresponding $S(\mathbf{q}, \Delta E)$ matched the ratio of hydrogen atoms in each system.

F. Elastic incoherent neutron scattering

The elastic scattering intensity, denoted as $S(\mathbf{q}, \Delta t)$, corresponds to the elastic peak within the dynamic structure factor. This intensity is conventionally normalized concerning the lowest temperature, typically ∼10 K, or with respect to the resolution function. It approximates the value of the intermediate scattering function as it decays to the resolution time of the instrument Δt [35,71]:

$$S(\mathbf{q}, \Delta t) \approx I_{\text{inc}}(\mathbf{q}, \Delta t) = \frac{1}{N}\sum_{j}^{N} b_{j,\text{inc}}^2 \langle \exp[-i\mathbf{q}\cdot\mathbf{r}_j(0)] \times \exp[i\mathbf{q}\cdot\mathbf{r}_j(\Delta t)]\rangle, \quad (5)$$

where N is the total number of atoms, $b_{j,\text{inc}}$ signifies the incoherent scattering length associated with a specific atom j, and $\mathbf{r}_j$ denotes the position vector of said atom. The brackets encapsulate an ensemble and orientation average, while $\mathbf{q}$ represents the scattering wave vector. Here, $I_{\text{inc}}(\mathbf{q}, \Delta t)$ elucidates self-correlations intrinsic to atomic motions.

The elastic scattering intensity is calculated by the convolution of the experimentally measured structural factor and the resolution function:

$$S(\mathbf{q}, \Delta E = 0) = \int S(\mathbf{q}, \Delta E)\cdot R(\mathbf{q}, 0 - \Delta E) d(\Delta E). \quad (6)$$

For the cell samples, the neutron scattering experiments of *E. coli*, 3DAC, and A501 were carried out using the backscattering Emu spectrometer at ANSTO in Australia with a resolution of ∼1 μeV, equivalent to a time scale of ∼1 ns. These experiments were designed to scrutinize the dynamics of the cellular proteome. The elastic scattering intensities $S(\mathbf{q}, \Delta t)$ for *E. coli*, 3DAC, and A501 were acquired over a temperature range spanning 4–30, 4–70, and 4−70 °C, respectively, during over a controlled heating process at a rate of 1.0 K/min. The $\mathbf{q}$ values of the collected data ranged from 0.27 to 1.97 Å^{-1}. A vanadium sample served as a reference for defining instrument resolution and correcting detector efficiency. The intensity data underwent corrections for sample container and buffer scattering, followed by normalization using vanadium scattering to generate $S(\mathbf{q}, \Delta t)$ as a temperature-dependent function for each sample. The sample containers were situated in a nitrogen exchange gas atmosphere to ensure a uniform temperature profile. Mean-squared displacement (MSD), $\langle x^2(\Delta t)\rangle$, were estimated utilizing a Gaussian approximation, where $S(\mathbf{q}, \Delta t) = \exp[-\frac{1}{6}\mathbf{q}^2\langle x^2(\Delta t)\rangle]$, in the $\mathbf{q}$ range from 1.30 to 1.97 Å^{-1}, corresponding to a spatial-temporal measurement window of a few Ångstroms in ∼1 ns.

For GFP and CYP119, $S(\mathbf{q}, \Delta t)$ datasets were collected across various forms, including dry proteins, H-protein + D_2O, and D-protein + H_2O, within the temperature range of ∼10–300 K during a controlled heating process at a rate of 1.0 K/min. These measurements were conducted employing the high flux backscattering spectrometer (HFBS) at the NIST Center for Neutron Research in the U.S., offering a resolution of ∼1 μeV. Meanwhile, CYP101 was examined in both dry and hydrated forms in D_2O under the same conditions. The energy resolution of HFBS approximates 1 μeV, corresponding to $\Delta t \sim 1$ ns. Given that samples were prepared for neutron transmission over 0.9, no correction for multiple scattering was applied, as the impact of multiple scattering can be considered negligible under these conditions [72]. The $\mathbf{q}$ range of our measurement spans from 0.36 to 1.75 Å^{-1}. MSD was determined utilizing the Gaussian approximation in the $\mathbf{q}$ range from 0.36 to 1.32 Å^{-1}.

G. Water sorption isothermal experiment

Multitemperature isotherms at 280, 288, 293, 298, and 303 K were conducted for GFP, LYS, and MYO using the MicrotacBEL BELSORP-max II apparatus at ShanghaiTech University, China. Preceding each adsorption measurement, a meticulous degassing procedure was implemented at room temperature overnight for all protein samples, ensuring the removal of moisture and other contaminants, facilitated by the Quantachrome FloVac system. Each adsorption-desorption cycle commenced from the dry state, with the sample exposed to water vapor until reaching a relative vapor pressure $p_r = p/p_0 \geqslant 0.9$. Here, p denotes the equilibrium water vapor pressure corresponding to a given temperature and hydration level (h), while p_0 signifies the saturated value. Subsequently, the p/p_0 values were systematically reduced to zero with step intervals ranging from 0.02 to 0.05. To prevent potential irreversible structural changes in the protein molecule induced by exhaustive drying [73], only the desorption isotherms within the p/p_0 range of 0.9–0.1 were considered for the analysis of the thermodynamic properties of the system.

The differential thermodynamic characterizing protein hydration can be deduced from the following equations:

$$\Delta G = RT\ln\frac{p}{p_0} \equiv RT\ln p_r, \quad (7)$$

$$\Delta H = -RT^2\left(\frac{d\ln p_r}{dT}\right)_h = 1000 \times R\left[\frac{d\ln p_r}{d\left(\frac{1000}{T}\right)}\right]_h, \quad (8)$$

$$\Delta S = -RT\left(\frac{d\ln p_r}{dT}\right)_h - R\ln p_r, \quad (9)$$

where R is the gas constant, and p and p_0 represent the experimental equilibrium water pressure and the saturation pressure of bulk water, respectively. Here, ΔG denotes the alteration in Gibbs free energy when a mole of water molecules is adsorbed onto the protein relative to the bulk water, and ΔH and ΔS correspond to the associated enthalpy and entropy changes. The van't Hoff plots, specifically $\ln p_r$ vs $1000/T$, exhibited linearity across all three systems within the hydration levels spanning from 0.1 to 0.3. This linearity suggests that ΔH is exclusively determined by h within the investigated hydration range. The enthalpy terms were assessed through linear fits, while the entropy terms were derived as the intercepts of the van't Hoff lines upon extrapolation to $1000/T = 0$ (see Fig. S3 in the Supplemental Material [61]).

III. RESULTS

A. Dynamics of proteome and the hydration water in living cells

In a preceding investigation, we focused on three microorganisms to assess the diffusionlike dynamics of the proteome within living cells [36]. The first microorganism *E. coli* is

a mesophilic bacterium with a growth temperature range of 21−49 °C and an optimal temperature of 37 °C [74]. The second microorganism is 3DAC, characterized as a thermophilic bacterium with a growth temperature range of 30−75 °C and an optimal temperature of 70 °C [55]. The third microorganism is A501, identified as a hyperthermophilic archaeon with a growth temperature range of 50−100 °C and an optimal temperature of 85 °C [56]. The overall compositions of these three cells exhibit minimal variation between cell types, with proteins constituting the most abundant dry weight cellular component (see Table S2 in the Supplemental Material [61]). This suggests that despite the sample being fully hydrogenated, proteins predominantly contribute to the neutron signal. Meanwhile, cellular water has minimal contribution within the time window accessible on Emu, a spectrometer for elastic neutron scattering, at a resolution of ∼1 μeV. Consequently, the neutron signals at Emu predominantly portray the self-diffusive dynamics of the average protein or proteome in the cytoplasm [35,75,76]. As illustrated in Fig. 2(a), the proteome in *E. coli* demonstrates the highest flexibility, succeeded by 3DAC, while the hyperthermophile exhibits the most rigid proteome. This outcome aligns with previous neutron experiments [35,76], where thermophiles exhibited greater macromolecular rigidity than mesophiles, indicating that proteins in thermophiles are more likely to possess stronger intramolecular interactions to adapt to higher temperatures.

Furthermore, our investigation encompasses an exploration of the diffusion dynamics of cellular water and biomacromolecules in the three microorganisms under study. Previous studies have indicated that QENS with a resolution of ∼15 μeV can reveal contributions to cellular dynamics categorized into four components: (i) very slow motions of biomacromolecules, (ii) slow diffusion of hydration water molecules, (iii) fast diffusion of water molecules beyond hydration shells, and (iv) localized motions of macromolecules and water molecules [37,38]. Considering that proteins constitute the majority of the dry weight cellular composition, and the size of most proteins (2–5 nm) [77] is much smaller than that of ribosomes (21 nm) [78], it is reasonable to assume that neutron signals from hydration water molecules are predominantly influenced by the hydration water surrounding the proteome. Therefore, we can reveal the diffusion dynamics of hydration water on proteins and water beyond hydration shells in living cells by using QENS at ∼15 μeV. Subsequently, QENS data at a resolution of 13 μeV were collected for 3DAC and A501 in the temperature range from 4 to 70 °C, while the dynamics of *E. coli* were probed from 4 to 30 °C. SAXS measurements indicated that no significant changes were observed within the temperature range examined for cellular dynamics, suggesting that the biomacromolecules remain structurally intact [79] (see Fig. S4 in the Supplemental Material [61]). Following the analytical method used in Ref. [38], we extracted the diffusion dynamics of hydration water molecules and the water molecules beyond the hydration shells from the QENS data (see Figs. S1 and S2 in the Supplemental Material [61]). Figure 2(b) illustrates a remarkably similar diffusion coefficient D_{bulklike} between water molecules beyond the hydration shells in different cells at various temperatures. These water molecules exhibited only slightly slower diffusion than bulk water, earning them the designation of bulklike water. Notably, the hydration water of the proteome in A501 exhibited the fastest diffusion, followed by that in 3DAC, while the hydration water of the proteome in *E. coli* moved most slowly [see Fig. 2(c)]. Our neutron experimental findings demonstrated that the hyperthermophilic A501 possessed the most rigid proteome and the most rapid diffusion of hydration water of the proteome, whereas the mesophilic *E. coli* exhibited the most flexible proteome and the slowest motion of hydration water of the proteome. The dynamics of the proteome and its hydration water exhibited an inverse correlation in these three microorganisms, wherein a less dynamic proteome corresponded to faster diffusion of its hydration water. Based on this observation, we postulated whether this inverse correlation between the dynamics of pro-

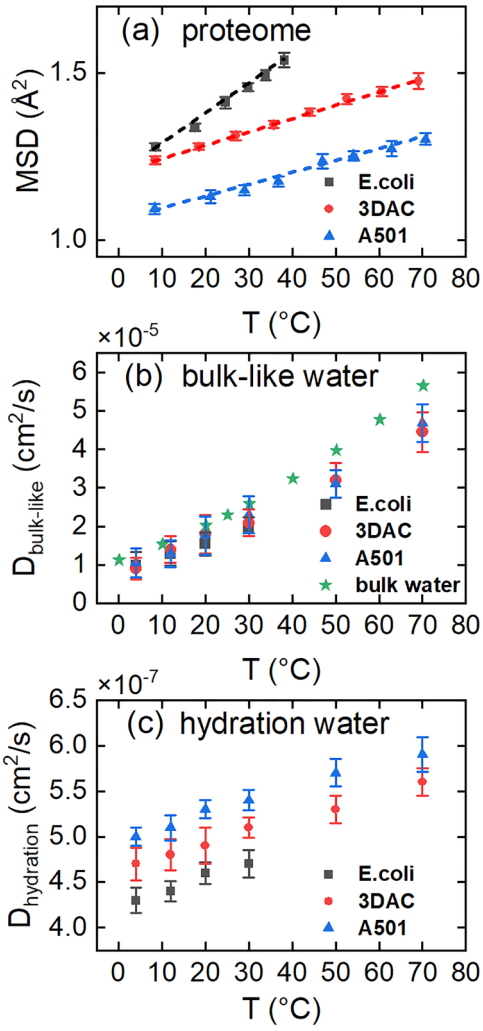

FIG. 2. Dynamics of proteome and cellular water in living cells. (a) Mean-squared displacement (MSD) of proteome in *E. coli* (black squares), 3DAC (red dots), and A501 (blue triangles) as a function of temperature. The data were extracted from Ref. [36] and replotted. (b) Diffusion coefficients D_{bulklike} of bulk water (green stars) and bulklike water in *E. coli* (black squares), 3DAC (red dots), and A501 (blue triangles) as a function of temperature. (c) Diffusion coefficients $D_{\text{hydration}}$ of hydration water in *E. coli* (black squares), 3DAC (red dots), and A501 (blue triangles) as a function of temperature. Error bars represent one standard deviation.

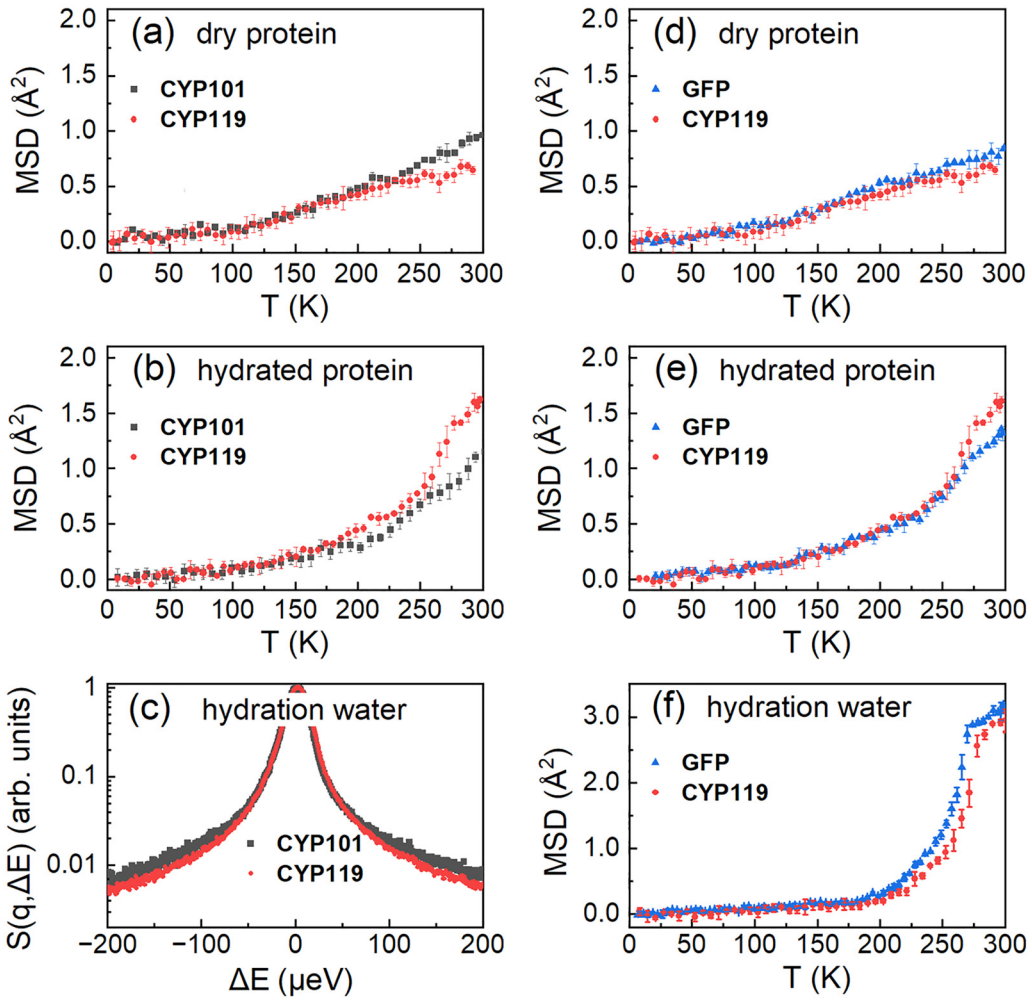

FIG. 3. Dynamics of CYP101, CYP119, green fluorescence protein (GFP), and their hydration water. Mean-squared displacements (MSDs) of CYP101 and CYP119 in the (a) dry and (b) hydrated forms as a function of temperature. (c) Quasielastic neutron scattering spectra of hydration water on CYP101 and CYP119 at OSIRIS with a resolution of 25.4 μeV at 280 K. Spectra in (c) were normalized to maximum peak intensity. The results of CYP101 and CYP119 are expressed as black squares and red dots, respectively. MSDs of GFP and CYP119 in the (d) dry and (e) hydrated forms as well as (f) the hydration water as a function of temperature. The results of GFP and CYP119 are presented as blue triangles and red dots, respectively. The elastic scattering intensity datasets were collected at HFBS with a resolution of ∼1 μeV. Error bars represent 1 standard deviation.

teome and its hydration water also holds for the correlation between the dynamics of a protein and its hydration water, i.e., a more flexible protein has slower hydration water. Also, it is noteworthy that a thermophilic protein can be more dynamic than a mesophilic protein [80,81]. This prompts us to pose a further question: Does the thermophilic protein with higher flexibility exhibit slower hydration water motions than that on a more rigid mesophilic protein?

B. Dynamics of proteins and their hydration water in the mesophilic and thermophilic proteins

To address this question, we opted to explore the diffusionlike dynamics of a mesophilic CYP101 in comparison with its thermophilic counterpart CYP119. Despite these two proteins sharing very similar secondary and tertiary structures (see Fig. S5 and Table S3 in the Supplemental Material [61]), their denaturation temperatures differ significantly, with a gap of ∼40 °C (50 °C for CYP101 vs 90 °C for CYP119) [80]. To assess the dynamics of both proteins, we conducted elastic neutron scattering experiments to determine the MSDs of the proteins in both dry and hydrated forms (H-protein + D_2O). As shown in Fig. 3(a), dry CYP101 is slightly more flexible than dry CYP119, while CYP119 demonstrates higher MSDs when hydrated across the temperature range from 200 to 300 K [see Fig. 3(b)]. For a quantitative analysis of the hydration water diffusion dynamics, we performed QENS on perdeuterated protein hydrated with H_2O, where the neutron signals predominantly capture the motion of hydration water [8]. As illustrated in Fig. 3(c), the quasielastic component of water on CYP101 at 280 K appears broader than that on CYP119, indicating increased mobility in the former, in contrast with the dynamics observed in the two proteins.

In addition, we chose another mesophilic protein GFP, with a structurally distinct profile from that of CYP119 (see Fig. S5

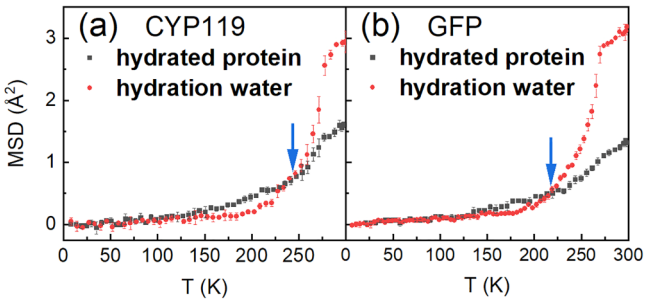

FIG. 4. Dynamics of protein and its hydration water for green fluorescence protein (GFP) and CYP119. (a) Mean-squared displacements (MSDs) of hydrated CYP119 (black squares) and its hydration water (red dots). (d) MSDs of hydrated GFP (black squares) and its hydration water (red dots). The blue arrows point out the temperatures for the dynamic separation between the proteins and their hydration water. Error bars represent one standard deviation.

and Table S3 in the Supplemental Material [61]), to juxtapose the dynamics of the protein and its hydration water with those of CYP119. As depicted in Figs. 3(d) and 3(e), GFP and CYP119 exhibit analogous dynamics in their dry form, while the hydrated CYP119 demonstrates greater flexibility than the hydrated GFP. In contrast with the dynamic features of the proteins, the hydration water moves more slowly around the thermophilic CYP119 than around the mesophilic GFP [see Fig. 3(f)]. These findings closely align with a previous report [29] emphasizing greater flexibility in IDPs than globular, folded proteins and more restricted water motions on the IDP surface (Figs. S6(a) and S6(b) in the Supplemental Material [61]). Moreover, the coupling effect between protein and water can be assessed by comparing the temperature dependence of their respective MSDs (Fig. 4). With increasing temperature, they closely track each other up to 250 K in the case of CYP119 but diverge at 220 K in the case of GFP. This suggests a tighter coupling with hydration-water dynamics for the thermophilic CYP119 than for the mesophilic GFP. Similar observations were made when comparing the protein-water coupling effect between an IDP and a folded protein (Figs. S6(c) and S6(d) in the Supplemental Material [61]). Based on these findings, we propose that a more dynamic protein is highly likely to correspond to less mobile hydration water due to their stronger coupling interactions.

It is noteworthy that, for both dry and hydrated proteins, the MSDs exhibit a sudden increase ∼100 K, which is associated with the rotation of methyl groups on the protein side chains (see Figs. S7(a) to S7(f) in the Supplemental Material [61]) [82,83]. However, in contrast with dry protein, the MSDs of hydrated proteins, including CYP101, CYP119, and GFP, rapidly increase ∼200 K, corresponding to the so called *dynamical transition* (see Figs. S7(d) to S7(f) in the Supplemental Material [61]) [84–87]. This transition has been attributed to the hydration effect, where the motion of the side chains of the protein is significantly driven by hydration water [84,88]. The MSDs of the hydration water for both CYP119 and GFP, as depicted in Figs. S7(g) and S7(h) in the Supplemental Material [61], also commence ∼200 K, corroborating the driving role of hydration water. Additionally, we can observe another transition in the MSDs of hydrated proteins, particularly for CYP119, ∼270 K. This could potentially be the impact of the phase transition of water on the protein dynamics [89].

C. Dynamics of proteins and their hydration water in three globular proteins with various structures

To examine our hypothesis, we conducted QENS experiments on three representative globular proteins: GFP, LYS, and MYO. These proteins manifest remarkable distinctions in their secondary and tertiary structures (see Fig. S5 and Table S3 in the Supplemental Material [61]), forming a gradient from a protein predominantly characterized by β sheets to one primarily constituted by an α helix. While both GFP and MYO exhibit a singular domain, LYS comprises two domains interconnected through a hinge region. The measured parameter in the QENS experiments is the dynamic structure factor, denoted as $S(\mathbf{q}, \Delta E)$, which elucidates the distribution of dynamical modes in the system across energy ΔE at a given $\mathbf{q}$. The explored energy range spans from a few microeletronvolts to 100 μeV, corresponding to temporal scales of 10–100 ps.

Here, $S(\mathbf{q}, \Delta E)$ datasets acquired at 280 K for the three proteins are illustrated in Fig. 1, with each protein examined in three distinct states: lyophilized in the dry state [Fig. 1(a)], hydrated in D_2O [Fig. 1(b)], and hydrated in H_2O [Fig. 1(c)]. For brevity, these states are referred to as dry H-protein, H-protein + D_2O, and H-protein + H_2O, respectively. The hydration levels of the latter two, denoted as h, are both 0.3 g water per gram protein, roughly corresponding to a monolayer of water enveloping the protein surface. Due to the neutron incoherent scattering cross-section of hydrogen atoms being an order of magnitude larger than the incoherent and coherent cross-sections of other elements, the recorded neutron signals predominantly depict the dynamics of hydrogen atoms in the system [8,41,90]. Consequently, Figs. 1(a)–1(c) delineate the diffusionlike dynamics of dry protein, the motions of hydrated protein, and the combined mobility of both protein and water in powder form, respectively. As depicted in Fig. 1(a), $S(\mathbf{q}, \Delta E)$ of the three dry samples are virtually indistinguishable, suggesting similar flexibility in the lyophilized state despite substantial differences in their structures. Upon hydration, $S(\mathbf{q}, \Delta E)$ of the three proteins (H-protein + D_2O) significantly broadens compared with that of the dry sample (Fig. S8 in the Supplemental Material [61]), signifying heightened protein dynamics upon hydration. More notably, $S(\mathbf{q}, \Delta E)$ of the three hydrated proteins differs [see Fig. 1(b)], with the quasielastic component being broadest for LYS and narrowest for GFP. Thus, the ranking of protein flexibility stands as $P_{\mathrm{LYS}} > P_{\mathrm{MYO}} > P_{\mathrm{GFP}}$ once they are hydrated by a monolayer of water. Here, the letter P denotes protein.

Notably, $S(\mathbf{q}, \Delta E)$ of the three proteins converges to an approximately indistinguishable profile when characterizing H-protein + H_2O, implying a close resemblance in the combined mobility of protein and water across different samples. By integrating Figs. 1(b) and 1(c), one can infer an inverse correlation between the mobility of hydration water and the flexibility of the protein, ensuring a comparable

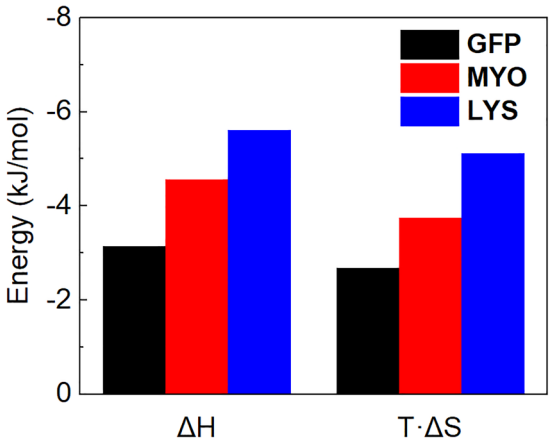

FIG. 5. Thermodynamic parameters of water sorption on three globular proteins. All thermodynamic parameters of green fluorescence protein (GFP), myoglobin (MYO), and lysozyme (LYS) were collected at the hydration level of 0.3 at 280 K. ΔH is the enthalpy change when one mole of water molecules adsorbed to protein surface by reference to bulk water at a given hydration level, and ΔS is the corresponding entropy change. The results of GFP, MYO, and LYS are expressed as black, red, and blue columns, respectively.

combined mobility in various systems. Consequently, the mobility of hydration water on these three proteins is expected to rank oppositely compared with the proteins, i.e., $W_{\mathrm{GFP}} > W_{\mathrm{MYO}} > W_{\mathrm{LYS}}$, where the letter W signifies hydration water. This is further substantiated by Fig. 1(d), where the subtraction of $S(\mathbf{q}, \Delta E)$ of H-protein + D_2O from that of H-protein + H_2O is employed to portray the diffusion dynamics of protein hydration water [designated as $S_{\mathrm{W}}(\mathbf{q}, \Delta E)$] [91], and the resulting $S_{\mathrm{W}}(\mathbf{q}, \Delta E)$ indeed exhibits the broadest profile for water on GFP and the narrowest for that on LYS.

D. Interaction strength between protein and its hydration water

In addition to investigating the diffusionlike/diffusion dynamics of protein and its hydration water, we undertook measurements to assess the interaction strength between these two components in the context of the three protein systems. Specifically, water sorption isothermal experiments were conducted to quantify the enthalpy and entropy changes, ΔH and ΔS, associated with water adsorption to the protein surface at $h = 0.3$, using bulk water as a reference [73,92]. A negative ΔH value signifies hydrophilic hydration [92], and a more negative ΔH indicates a stronger attractive interaction between the protein and water [93]. As depicted in Fig. 5, ΔH values for all three proteins are negative, with the absolute values ranking as $P_{\mathrm{LYS}} > P_{\mathrm{MYO}} > P_{\mathrm{GFP}}$. This indicates that LYS exhibits the highest affinity for water, while GFP displays the least. Additionally, ΔS represents the entropy loss of water upon adsorption to the protein surface, with a higher ΔS value indicating that water experiences a greater restriction in freedom upon adsorption. Figure 5 illustrates that the entropy loss of protein hydration water follows the ranking $W_{\mathrm{LYS}} > W_{\mathrm{MYO}} > W_{\mathrm{GFP}}$. Consequently, the mobility of the hydration water should exhibit an opposite ranking, aligning precisely with the observations in the neutron scattering experiments [Fig. 1(d)].

By combining the outcomes of neutron scattering experiments with water sorption isothermal data for the three protein systems, it can be inferred that a heightened protein-water interaction contributes to increased protein mobility while concurrently diminishing the mobility of its hydration water. Within the probed timeframe, water molecules exhibit considerably greater mobility than protein residues. Following the principles of the second law of thermodynamics, when a swifter entity encounters a slower one, the mobility of the former is inherently transferred to the latter through their reciprocal interaction. Consequently, hydration inevitably curtails the mobility of protein hydration water compared with bulk water [8], concurrently augmenting protein flexibility concerning the dry state (Fig. S8 in the Supplemental Material [61]). A more robust interaction intensifies protein flexibility by further constraining water mobility, providing a rational explanation for the observations in Figs. 1 and 5. In this paper, we unveil a hitherto unexplored mechanism governing protein-water coupling, wherein the protein and its hydration water collectively form a dynamically united entity. Furthermore, the mobility of these two components can be reciprocally adjusted by altering their interaction strength.

IV. DISCUSSION

In this investigation, neutron scattering experiments were conducted to understand the diffusionlike/diffusion dynamics of proteins and water in a systematic way, by choosing proteins of different structures and characterized by varying thermostability as well as living cells with distinct growth temperatures. The outcomes reveal a discernible inverse correlation between the flexibility of hydrated proteins and the mobility of their hydration water. Subsequent water sorption isothermal experiments elucidated that samples exhibiting higher protein flexibility and lower water mobility concurrently manifest a greater attractive interaction energy between the protein and water. The experimental results indicate that the diffusionlike dynamics of the various dry proteins are consistent, and the diffusionlike dynamics of the protein-water combinations are indistinguishable (Fig. 1). However, the individual dynamics of each component, protein and its hydration water, are observed to change with the interactions between them. These experimental insights collectively propose a conceptual framework regarding the dynamics of protein-water systems, positing that these two components integrate into a unified dynamic entity. Within this entity, the mobility of water is transferred to the enclosed protein molecule through protein-water interaction, with stronger interactions resulting in enhanced transportation. This finding holds fundamental significance for comprehending the physical underpinnings of protein flexibility in the hydrated state and its modulation across different biological species. Furthermore, our results harmonize with the theoretical framework proposed by Mukherjee *et al.* [22], suggesting that an increase in protein energy corresponds to a decrease in water energy in accordance with the law of energy conservation. Given that the dynamics of hydration water are dictated by the interaction strength with the protein rather than the protein structure, our findings offer an explication for the accelerated diffusive motion of hydrated water on an IDP ($A\beta_{1-42}$) compared

with water molecules on a globular protein (ubiquitin) [33]. Additionally, notwithstanding the potential decoupling of the dynamics of internal residues in proteins from the surrounding matrix [27,28], we posit a delicately balanced reciprocation between the dynamics of the protein and its hydration water when treating all residues in the protein as an ensemble.

More importantly, as illustrated by the findings in Ref. [80], the heightened thermal stability of CYP119 arises from the increased dynamism of the protein in its folded state. This enhanced dynamics reduces the entropy gain during denaturation, consequently elevating the unfolding free energy barrier. In this paper, we introduce a complementary perspective, contending that the enhanced mobility of CYP119 in its native state is attributed to a stronger interaction with water rather than its intrinsic structure. This implies that, through smart design of amino acid sequences, nature has the capacity to finely regulate the interaction strength between water and distinct proteins within a given enzyme family. This regulation leads to substantial dynamic distinctions among these proteins without necessitating significant alterations to their structures. The preservation of protein structures within an enzyme family is of paramount importance to ensure the execution of specific bioactivities, while the introduction of dynamical diversity may prove vital for adapting a particular protein to a specific environmental context. For instance, while CYP101 operates under ambient conditions, CYP119 functions in hot springs with temperatures exceeding 80 °C [67].

Furthermore, the observed inverse correlation between the dynamics of protein and its hydration water aligns with the intricate interplay between the proteome and its hydration water within living cells. The proposed higher rigidity of the proteome in thermophiles has been suggested as an adaptive strategy to cope with elevated temperatures [35,76]. While it is reasonable to anticipate that the hydration water surrounding the proteome in thermophiles is more dynamic than that in mesophiles, additional investigations are imperative to elucidate the specific role of the enhanced diffusion dynamics of hydration water in the proteome during the thermal adaptation of thermophiles.

In summary, in this paper, we employ neutron scattering techniques to comprehensively characterize the dynamics of proteins and their hydration water in diverse systems. We unveil a reciprocal coupling effect governing the dynamics of proteins and their hydration water across proteins exhibiting distinct thermostability and structural variations. Furthermore, this coupling phenomenon extends to the dynamics of the proteome and its hydration water in living cells, illustrating that a more flexible proteome corresponds to constrained motions of its hydration water. Our water sorption isothermal experiments elucidate that the weaker interaction between protein and its hydration water leads to decreased protein flexibility and increased water mobility, emphasizing the dynamic synergy between protein and its hydration water. It is worth noting that structural flexibility plays a pivotal role in designing proteins for specific ligand binding, adapting to extreme environments (e.g., high temperature, pressure, or pH), and targeted therapeutic applications. Through a focused investigation of thermophilic and mesophilic cytochrome P450s, in this paper, we demonstrate the capacity of nature to modulate protein-water interaction strength, thereby altering protein flexibility without significant structural modifications. This tunability is crucial for preserving the functionality of diverse proteins within a given biological context while enabling adaptation to challenging environments. Consequently, in this paper, we introduce a potential avenue for designing proteins with tailored flexibility for applications in medical or industrial settings through strategic mutations that adjust biomolecular interactions with water. The profound insights into the dynamic interplay between proteins and their hydration water presented herein hold promise to engage a broad audience, including those in food science [94], personal care [95,96], pharmaceutical industries [97], and scientific communities interested in protein folding, binding, and recognition [2,3]. It is our expectation that these findings will contribute to a deeper understanding across diverse scientific and industrial domains focused on proteins and their hydration water.

Data are available online [98].

ACKNOWLEDGMENTS

This paper was supported by the National Natural Science Foundation of China (Grants No. 12204302 and No. 42106087), the Shanghai Pujiang Program (Grant No. 22PJ1406900), the Startup Fund for Young Faculty at SJTU, the Oceanic Interdisciplinary Program of SJTU (Project No. SL2022MS018), the Natural Science Foundation of Shanghai (Grant No. 23ZR1431700), SJTU Scientific and Technological Innovation Funds (21X010200843), the Student Innovation Center at SJTU. H.O. and Q.Z. acknowledge the support of Center for Structural Molecular Biology (FWPERKP291) funded by the U.S. Department of Energy Office of Biological and Environmental Research. The authors are grateful for the support from the Analytical Instrumentation Center (Grant No. SPST-AIC10112914), SPST, ShanghaiTech University. Access to the HFBS was provided by the Center for High Resolution Neutron Scattering, a partnership between the National Institute of Standards and Technology and the National Science Foundation under Agreement No. DMR-2010792. The neutron experiment at the Materials and Life Science Experimental Facility of the J-PARC was performed under two user programs (Proposals No. 2019A0020 and No. 2022B0182). Experiments at the ISIS Neutron and Muon Source were supported by a beamtime allocation RB1800112 from the Science and Technology Facilities Council. We acknowledge the support of the Australian Centre for Neutron Scattering (ACNS), ANSTO, and the Australian Government through the National Collaborative Research Infrastructure Strategy, in supporting the neutron research infrastructure used in this paper via ACNS Proposal No. P9325. We would like to thank Dr. Na Li from BL19U2 beamline of SSRF for the help with synchrotron SAXS measurements on No. 2022-NFPS-PT-007003.

Z.L., W.Z., and L.H. designed and supervised the project. Y.Y., X.C., Z.L., and L.Z. prepared the samples for neutron scattering and SAXS and performed the measurements. J.H. offered the CYP proteins, while H.O. and Q.Z. provided the GFP proteins. Q.T. and W.Z. prepared the living cell samples. T.Y. contributed to the QENS experiments at DNA at J-PARC

in Japan, and V.G.S. assisted the quasielastic neutron scan at OSIRIS at ISIS in the UK. M.T. supported the elastic neutron scattering measurements at HFBS at NIST in the U.S., and N.R.S. performed the elastic neutron scan on cell samples at Emu at ANSTO in Australia. N.L. assisted the SAXS experiments at BL19U2 at SSRF in China. L.L. conducted the water adsorption test at ShanghaiTech University in China. Y.Y., X.C., X.X., Z.L., W.Z., and L.H. wrote the manuscript.

Certain commercial equipment, instruments, or materials are identified in this paper to specify the experimental procedure adequately. Such identification is not intended to imply recommendation or endorsement by NIST.

The authors declare no competing interests.

[1] P. Ball, Water as an active constituent in cell biology, Chem. Rev. **108**, 74 (2008).

[2] M.-C. Bellissent-Funel, A. Hassanali, M. Havenith, R. Henchman, P. Pohl, F. Sterpone, D. van der Spoel, Y. Xu, and A. E. Garcia, Water determines the structure and dynamics of proteins, Chem. Rev. **116**, 7673 (2016).

[3] Y. Levy and J. N. Onuchic, Water mediation in protein folding and molecular recognition, Annu. Rev. Biophys. Biomol. Struct. **35**, 389 (2006).

[4] N. V. Nucci, M. S. Pometun, and A. J. Wand, Site-resolved measurement of water-protein interactions by solution NMR, Nat. Struct. Mol. Biol. **18**, 245 (2011).

[5] E. Persson and B. Halle, Cell water dynamics on multiple time scales, Proc. Natl. Acad. Sci. USA **105**, 6266 (2008).

[6] M. Reuhl and M. Vogel, Temperature-dependent dynamics at protein-solvent interfaces, J. Chem. Phys. **157**, 074705 (2022).

[7] G. Schirò, Y. Fichou, F.-X. Gallat, K. Wood, F. Gabel, M. Moulin, M. Härtlein, M. Heyden, J.-P. Colletier, A. Orecchini *et al.*, Translational diffusion of hydration water correlates with functional motions in folded and intrinsically disordered proteins, Nat. Commun. **6**, 6490 (2015).

[8] P. Tan, Y. Liang, Q. Xu, E. Mamontov, J. Li, X. Xing, and L. Hong, Gradual crossover from subdiffusion to normal diffusion: A many-body effect in protein surface water, Phys. Rev. Lett. **120**, 248101 (2018).

[9] G. Schirò, Y. Fichou, A. P. S. Brogan, R. Sessions, W. Lohstroh, M. Zamponi, G. J. Schneider, F. X. Gallat, A. Paciaroni, D. J. Tobias *et al.*, Diffusivelike motions in a solvent-free protein-polymer hybrid, Phys. Rev. Lett. **126**, 088102 (2021).

[10] M. T. F. Telling, L. Clifton, J. Combet, B. Frick, S. Howells, and V. G. Sakai, Lyophilised protein dynamics: More than just methyls? Soft Matter **8**, 9529 (2012).

[11] S. H. Chen, L. Liu, E. Fratini, P. Baglioni, A. Faraone, and E. Mamontov, Observation of fragile-to-strong dynamic crossover in protein hydration water, Proc. Natl. Acad. Sci. USA **103**, 9012 (2006).

[12] J. Yang, Y. Wang, L. Wang, and D. Zhong, Mapping hydration dynamics around a β-barrel protein, J. Am. Chem. Soc. **139**, 4399 (2017).

[13] Y. Qin, L. Wang, and D. Zhong, Dynamics and mechanism of ultrafast water–protein interactions, Proc. Natl. Acad. Sci. USA **113**, 8424 (2016).

[14] S. Arya, A. K. Singh, K. Bhasne, P. Dogra, A. Datta, P. Das, and S. Mukhopadhyay, Femtosecond hydration map of intrinsically disordered α-synuclein, Biophys. J. **114**, 2540 (2018).

[15] H. Frauenfelder, G. Chen, J. Berendzen, P. W. Fenimore, H. Jansson, B. H. McMahon, I. R. Stroe, J. Swenson, and R. D. Young, A unified model of protein dynamics, Proc. Natl. Acad. Sci. USA **106**, 5129 (2009).

[16] P. W. Fenimore, H. Frauenfelder, B. H. McMahon, and F. G. Parak, Slaving: Solvent fluctuations dominate protein dynamics and functions, Proc. Natl. Acad. Sci. USA **99**, 16047 (2002).

[17] S. Khodadadi and A. P. Sokolov, Protein dynamics: From rattling in a cage to structural relaxation, Soft Matter **11**, 4984 (2015).

[18] J. T. King and K. J. Kubarych, Site-specific coupling of hydration water and protein flexibility studied in solution with ultrafast 2D-IR spectroscopy, J. Am. Chem. Soc. **134**, 18705 (2012).

[19] G. Sieler and R. Schweitzer-Stenner, The amide I mode of peptides in aqueous solution involves vibrational coupling between the peptide group and water molecules of the hydration shell, J. Am. Chem. Soc. **119**, 1720 (1997).

[20] S. Ebbinghaus, S. J. Kim, M. Heyden, X. Yu, U. Heugen, M. Gruebele, D. M. Leitner, and M. Havenith, An extended dynamical hydration shell around proteins, Proc. Natl. Acad. Sci. USA **104**, 20749 (2007).

[21] G. Giubertoni, L. Feng, K. Klein, G. Giannetti, L. Rutten, Y. Choi, A. van der Net, G. Castro-Linares, F. Caporaletti, D. Micha *et al.*, Elucidating the role of water in collagen self-assembly by isotopically modulating collagen hydration, Proc. Natl. Acad. Sci. USA **121**, e2313162121 (2024).

[22] S. Mukherjee, S. Mondal, and B. Bagchi, Mechanism of solvent control of protein dynamics, Phys. Rev. Lett. **122**, 058101 (2019).

[23] S. Mukherjee, S. Mondal, S. Acharya, and B. Bagchi, Tug-of-war between internal and external frictions and viscosity dependence of rate in biological reactions, Phys. Rev. Lett. **128**, 108101 (2022).

[24] K. Wood, A. Frölich, A. Paciaroni, M. Moulin, M. Härtlein, G. Zaccai, D. J. Tobias, and M. Weik, Coincidence of dynamical transitions in a soluble protein and its hydration water: Direct measurements by neutron scattering and MD simulations, J. Am. Chem. Soc. **130**, 4586 (2008).

[25] F. Sterpone, G. Stirnemann, and D. Laage, Magnitude and molecular origin of water slowdown next to a protein, J. Am. Chem. Soc. **134**, 4116 (2012).

[26] H. Frauenfelder, P. W. Fenimore, G. Chen, and B. H. McMahon, Protein folding is slaved to solvent motions, Proc. Natl. Acad. Sci. USA **103**, 15469 (2006).

[27] B. S. Marques, M. A. Stetz, C. Jorge, K. G. Valentine, A. J. Wand, and N. V. Nucci, Protein conformational entropy is not slaved to water, Sci. Rep. **10**, 17587 (2020).

[28] Y.-H. Kuo and Y.-W. Chiang, Slow dynamics around a protein and its coupling to solvent, ACS Cent. Sci. **4**, 645 (2018).

[29] F. X. Gallat, A. Laganowsky, K. Wood, F. Gabel, L. van Eijck, J. Wuttke, M. Moulin, M. Härtlein, D. Eisenberg, J. P. Colletier *et al.*, Dynamical coupling of intrinsically disordered proteins

and their hydration water: Comparison with folded soluble and membrane proteins, Biophys. J. **103**, 129 (2012).

[30] K. M. Reid, H. Poudel, and D. M. Leitner, Dynamics of hydrogen bonds between water and intrinsically disordered and structured regions of proteins, J. Phys. Chem. B **127**, 7839 (2023).

[31] K. M. Reid, A. K. Singh, C. R. Bikash, J. Wei, Y. Tal-Gan, N. Q. Vinh, and D. M. Leitner, The origin and impact of bound water around intrinsically disordered proteins, Biophys. J. **121**, 540 (2022).

[32] P. Rani and P. Biswas, Local structure and dynamics of hydration water in intrinsically disordered proteins, J. Phys. Chem. B **119**, 10858 (2015).

[33] J. C. Jose, P. Khatua, N. Bansal, N. Sengupta, and S. Bandyopadhyay, Microscopic hydration properties of the $A\beta_{1-42}$ peptide monomer and the globular protein ubiquitin: A comparative molecular dynamics study, J. Phys. Chem. B **118**, 11591 (2014).

[34] J. S. Gardner, G. Ehlers, A. Faraone, and V. García Sakai, High-resolution neutron spectroscopy using backscattering and neutron spin-echo spectrometers in soft and hard condensed matter, Nat. Rev. Phys. **2**, 103 (2020).

[35] M. Tehei, B. Franzetti, D. Madern, M. Ginzburg, B. Z. Ginzburg, M. T. Giudici-Orticoni, M. Bruschi, and G. Zaccai, Adaptation to extreme environments: Macromolecular dynamics in bacteria compared *in vivo* by neutron scattering, EMBO Rep. **5**, 66 (2004).

[36] W. Zhao, B. Zhong, L. Zheng, P. Tan, Y. Wang, H. Leng, N. de Souza, Z. Liu, L. Hong, and X. Xiao, Proteome-wide 3D structure prediction provides insights into the ancestral metabolism of ancient archaea and bacteria, Nat. Commun. **13**, 7861 (2022).

[37] M. Salvador-Castell, M. Golub, N. Martinez, J. Ollivier, J. Peters, and P. Oger, The first study on the impact of osmolytes in whole cells of high temperature-adapted microorganisms, Soft Matter **15**, 8381 (2019).

[38] M. P. M. Marques, A. L. M. Batista de Carvalho, V. G. Sakai, L. Hatter, and L. A. E. Batista de Carvalho, Intracellular water—An overlooked drug target? Cisplatin impact in cancer cells probed by neutrons, Phys. Chem. Chem. Phys. **19**, 2702 (2017).

[39] M. Jasnin, M. Moulin, M. Haertlein, G. Zaccai, and M. Tehei, Down to atomic-scale intracellular water dynamics, EMBO Rep. **9**, 543 (2008).

[40] N. Martinez, G. Michoud, A. Cario, J. Ollivier, B. Franzetti, M. Jebbar, P. Oger, and J. Peters, High protein flexibility and reduced hydration water dynamics are key pressure adaptive strategies in prokaryotes, Sci. Rep. **6**, 32816 (2016).

[41] Y. Ye, L. Zheng, L. Hong, V. García Sakai, N. R. de Souza, D. Teng, B. Wu, Y. Xu, J. Cai, and Z. Liu, Direct observation of the mutual coupling effect in the protein-water-glycerol mixture by combining neutron scattering and selective deuteration, J. Phys. Chem. B **128**, 405 (2024).

[42] M. C. Bellissent-Funel, J. Teixeira, S. H. Chen, B. Dorner, H. D. Middendorf, and H. L. Crespi, Low-frequency collective modes in dry and hydrated proteins, Biophys. J. **56**, 713 (1989).

[43] A. Paciaroni, A. Orecchini, M. Haertlein, M. Moulin, V. Conti Nibali, A. De Francesco, C. Petrillo, and F. Sacchetti, Vibrational collective dynamics of dry proteins in the terahertz region, J. Phys. Chem. B **116**, 3861 (2012).

[44] K. Yoshida, H. Uchiyama, and T. Yamaguchi, Structure and dynamical properties of hydrated F-actin investigated by x-ray scattering, J. Mol. Liq **291**, 111265 (2019).

[45] F. Sacchetti, J. B. Suck, C. Petrillo, and B. Dorner, Brillouin neutron scattering in heavy water: Evidence for two-mode collective dynamics, Phys. Rev. E **69**, 061203 (2004).

[46] E. Pontecorvo, M. Krisch, A. Cunsolo, G. Monaco, A. Mermet, R. Verbeni, F. Sette, and G. Ruocco, High-frequency longitudinal and transverse dynamics in water, Phys. Rev. E **71**, 011501 (2005).

[47] G. Ruocco, F. Sette, U. Bergmann, M. Krisch, C. Masciovecchlo, V. Mazzacurati, G. Signorelli, and R. Verbeni, Equivalence of the sound velocity in water and ice at mesoscopic wavelengths, Nature (London) **379**, 521 (1996).

[48] J. Teixeira, M. C. Bellissent-Funel, S. H. Chen, and B. Dorner, Observation of new short-wavelength collective excitations in heavy water by coherent inelastic neutron scattering, Phys. Rev. Lett. **54**, 2681 (1985).

[49] A. Orecchini, A. Paciaroni, A. D. Francesco, C. Petrillo, and F. Sacchetti, Collective dynamics of protein hydration water by Brillouin neutron spectroscopy, J. Am. Chem. Soc. **131**, 4664 (2009).

[50] H. Urabe, Y. Tominaga, and K. Kubota, Experimental evidence of collective vibrations in DNA double helix (Raman spectroscopy), J. Chem. Phys. **78**, 5937 (1983).

[51] S. Cocco and R. Monasson, Theoretical study of collective modes in DNA at ambient temperature, J. Chem. Phys. **112**, 10017 (2000).

[52] G. D'Angelo, V. C. Nibali, U. Wanderlingh, C. Branca, A. De Francesco, F. Sacchetti, C. Petrillo, and A. Paciaroni, Multiple interacting collective modes and phonon gap in phospholipid membranes, J. Phys. Chem. Lett. **9**, 4367 (2018).

[53] D. Soloviov, Y. Q. Cai, D. Bolmatov, A. Suvorov, K. Zhernenkov, D. Zav'yalov, A. Bosak, H. Uchiyama, and M. Zhernenkov, Functional lipid pairs as building blocks of phase-separated membranes, Proc. Natl. Acad. Sci. USA **117**, 4749 (2020).

[54] F. Sebastiani, A. Orecchini, A. Paciaroni, M. Jasnin, G. Zaccai, M. Moulin, M. Haertlein, A. De Francesco, C. Petrillo, and F. Sacchetti, Collective THz dynamics in living *Escherichia coli* cells, Chem. Phys. **424**, 84 (2013).

[55] H. Leng, Y. Wang, W. Zhao, S. M. Sievert, and X. Xiao, Identification of a deep-branching thermophilic clade sheds light on early bacterial evolution, Nat. Commun. **14**, 4354 (2023).

[56] W. Zhao, X. Zeng, and X. Xiao, *Thermococcus eurythermalis* sp. nov., a conditional piezophilic, hyperthermophilic archaeon with a wide temperature range for growth, isolated from an oil-immersed chimney in the Guaymas Basin, Int. J. Syst. Evol. Microbiol. **65**, 30 (2015).

[57] Y. Miao, Z. Yi, C. Cantrell, D. C. Glass, J. Baudry, N. Jain, and J. C. Smith, Coupled flexibility change in cytochrome P450cam substrate binding determined by neutron scattering, NMR, and molecular dynamics simulation, Biophys. J. **103**, 2167 (2012).

[58] F. Meilleur, M.-T. Dauvergne, I. Schlichting, and D. A. A. Myles, Production and x-ray crystallographic analysis of fully deuterated cytochrome P450cam, Acta Crystallogr. D: Struct. Biol. **61**, 539 (2005).

[59] J. D. Nickels, H. O'Neill, L. Hong, M. Tyagi, G. Ehlers, K. L. Weiss, Q. Zhang, Z. Yi, E. Mamontov, J. C. Smith *et al.*,

Dynamics of protein and its hydration water: Neutron scattering studies on fully deuterated GFP, Biophys. J. **103**, 1566 (2012).

[60] A. Nidriche, M. Moulin, P. Oger, J. R. Stewart, L. Mangin-Thro, W. Schmidt, G. Kneller, and J. Peters, Impact of isotopic exchange on hydrated protein dynamics revealed by polarized neutron scattering, PRX Life **2**, 013005 (2024).

[61] See Supplemental Material at http://link.aps.org/supplemental/10.1103/PhysRevResearch.6.033316 for details about QENS spectra and fitting curves of cells, FWHM vs q^2 from QENS fitting, van't Hoff plots of water sorption on three globular proteins, SAXS curves of cells, structures of selected globular proteins, dynamics of hydrated Tau and MBP as well as their hydration water, transitions observed in the MSDs of proteins and hydration water, comparisons of dynamic structure factors between dry and hydrated proteins, the sample preparation for quasi-elastic and elastic neutron scattering experiments, the relative dry weight of protein, DNA and RNA in cells, and the relative content of various secondary structures in each globular protein, which includes Refs. [29,66–70].

[62] J. B. Hopkins, BIOXTAS RAW 2: New developments for a free open-source program for small-angle scattering data reduction and analysis, J. Appl. Crystallogr. **57**, 194 (2024).

[63] D. Laage, Reinterpretation of the liquid water quasi-elastic neutron scattering spectra based on a nondiffusive jump reorientation mechanism, J. Phys. Chem. B **113**, 2684 (2009).

[64] J. J. Ullo, Molecular-dynamics study of translational motions in water as probed through quasielastic neutron scattering, Phys. Lett. A **36**, 816 (1987).

[65] O. Arnold, J. C. Bilheux, J. M. Borreguero, A. Buts, S. I. Campbell, L. Chapon, M. Doucet, N. Draper, R. Ferraz Leal, M. A. Gigg *et al.*, MANTID—Data analysis and visualization package for neutron scattering and μSR experiments, Nucl. Instrum. Methods Phys. Res. A **764**, 156 (2014).

[66] K. Harada, K. Sakurai, K. Ikemura, T. Ogura, S. Hirota, H. Shimada, and T. Hayashi, Evaluation of the functional role of the heme-6-propionate side chain in cytochrome P450cam, J. Am. Chem. Soc. **130**, 432 (2008).

[67] S.-Y. Park, K. Yamane, S.-i. Adachi, Y. Shiro, K. E. Weiss, S. A. Maves, and S. G. Sligar, Thermophilic cytochrome P450 (CYP119) from *Sulfolobus solfataricus*: High resolution structure and functional properties, J. Inorg. Biochem. **91**, 491 (2002).

[68] K. Brejc, T. K. Sixma, P. A. Kitts, S. R. Kain, R. Y. Tsien, M. Ormö, and S. J. Remington, Structural basis for dual excitation and photoisomerization of the *Aequorea victoria* green fluorescent protein, Proc. Natl. Acad. Sci. USA **94**, 2306 (1997).

[69] P. J. Artymiuk, C. C. F. Blake, D. W. Rice, and K. S. Wilson, The structures of the monoclinic and orthorhombic forms of hen egg-white lysozyme at 6 Å resolution, Acta Cryst. B **38**, 778 (1982).

[70] H.-P. Hersleth, T. Uchida, Å. K. Røhr, T. Teschner, V. Schuönemann, T. Kitagawa, A. X. Trautwein, C. H. Goörbitz, and K. K. Andersson, Crystallographic and spectroscopic studies of peroxide-derived myoglobin compound II and occurrence of protonated FeIV-O, J. Biol. Chem. **282**, 23372 (2007).

[71] D. Bicout, F. Gabel, U. Lehnert, M. Tehei, M. Weik, and G. Zaccai, Protein dynamics studied by neutron scattering, Q. Rev. Biophys. **35**, 327 (2002).

[72] S. Khodadadi, J. H. Roh, A. Kisliuk, E. Mamontov, M. Tyagi, S. A. Woodson, R. M. Briber, and A. P. Sokolov, Dynamics of biological macromolecules: Not a simple slaving by hydration water, Biophys. J. **98**, 1321 (2010).

[73] M. Lüscher-mattli and M. Rüegg, Thermodynamic functions of biopolymer hydration. I. Their determination by vapor pressure studies, discussed in an analysis of the primary hydration process, Biopolymers **21**, 403 (1982).

[74] M. Ferrer, T. N. Chernikova, M. M. Yakimov, P. N. Golyshin, and K. N. Timmis, Chaperonins govern growth of *Escherichia coli* at low temperatures, Nat. Biotechnol. **21**, 1267 (2003).

[75] D. Di Bari, S. Timr, M. Guiral, M.-T. Giudici-Orticoni, T. Seydel, C. Beck, C. Petrillo, P. Derreumaux, S. Melchionna, F. Sterpone *et al.*, Diffusive dynamics of bacterial proteome as a proxy of cell death, ACS Cent. Sci. **9**, 93 (2023).

[76] B. Caviglia, D. Di Bari, S. Timr, M. Guiral, M.-T. Giudici-Orticoni, C. Petrillo, J. Peters, F. Sterpone, and A. Paciaroni, Decoding the role of the global proteome dynamics for cellular thermal stability, J. Phys. Chem. Lett. **15**, 1435 (2024).

[77] H. P. Erickson, Size and shape of protein molecules at the nanometer level determined by sedimentation, gel filtration, and electron microscopy, Biol. Proced. Online **11**, 32 (2009).

[78] B. S. Schuwirth, M. A. Borovinskaya, C. W. Hau, W. Zhang, A. Vila-Sanjurjo, J. M. Holton, and J. H. D. Cate, Structures of the bacterial ribosome at 3.5 Å resolution, Science **310**, 827 (2005).

[79] A. R. von Gundlach, V. M. Garamus, T. M. Willey, J. Ilavsky, K. Hilpert, and A. Rosenhahn, Use of small-angle x-ray scattering to resolve intracellular structure changes of *Escherichia coli* cells induced by antibiotic treatment, J. Appl. Cryst. **49**, 2210 (2016).

[80] Z. Liu, S. Lemmonds, J. Huang, M. Tyagi, L. Hong, and N. Jain, Entropic contribution to enhanced thermal stability in the thermostable P450 CYP119, Proc. Natl. Acad. Sci. USA **115**, E10049 (2018).

[81] F. Jiang, J. Bian, H. Liu, S. Li, X. Bai, L. Zheng, S. Jin, Z. Liu, G.-Y. Yang, and L. Hong, Creatinase: Using increased entropy to improve the activity and thermostability, J. Phys. Chem. B **127**, 2671 (2023).

[82] L. Hong, D. C. Glass, J. D. Nickels, S. Perticaroli, Z. Yi, M. Tyagi, H. O'Neill, Q. Zhang, A. P. Sokolov, and J. C. Smith, Elastic and conformational softness of a globular protein, Phys. Rev. Lett. **110**, 028104 (2013).

[83] J. H. Roh, J. E. Curtis, S. Azzam, V. N. Novikov, I. Peral, Z. Chowdhuri, R. B. Gregory, and A. P. Sokolov, Influence of hydration on the dynamics of lysozyme, Biophys. J. **91**, 2573 (2006).

[84] J. H. Roh, V. N. Novikov, R. B. Gregory, J. E. Curtis, Z. Chowdhuri, and A. P. Sokolov, Onsets of anharmonicity in protein dynamics, Phys. Rev. Lett. **95**, 038101 (2005).

[85] J. A. Rupley and G. Careri, Protein hydration and function, in *Advances in Protein Chemistry*, edited by C. B. Anfinsen, F. M. Richards, J. T. Edsall, and D. S. Eisenberg (Academic Press, San Diego, 1991), Vol. 41, p. 37.

[86] W. Doster, S. Cusack, and W. Petry, Dynamical transition of myoglobin revealed by inelastic neutron scattering, Nature (London) **337**, 754 (1989).

[87] G. Zaccai, How soft is a protein? A protein dynamics force constant measured by neutron scattering, Science **288**, 1604 (2000).

[88] G. Caliskan, R. M. Briber, D. Thirumalai, V. Garcia-Sakai, S. A. Woodson, and A. P. Sokolov, Dynamic transition in tRNA is solvent induced, J. Am. Chem. Soc. **128**, 32 (2006).

[89] A. Panagopoulou, A. Kyritsis, A.-M. Aravantinou, D. Nanopoulos, R. S. i Serra, J. L. Gómez Ribelles, N. Shinyashiki, and P. Pissis, Glass transition and dynamics in lysozyme-water mixtures over wide ranges of composition, Food Biophys. **6**, 199 (2011).

[90] L. Zheng, Z. Liu, Q. Zhang, S. Li, J. Huang, L. Zhang, B. Zan, M. Tyagi, H. Cheng, T. Zuo *et al.*, Universal dynamical onset in water at distinct material interfaces, Chem. Sci. **13**, 4341 (2022).

[91] S. Perticaroli, G. Ehlers, C. B. Stanley, E. Mamontov, H. O'Neill, Q. Zhang, X. Cheng, D. A. A. Myles, J. Katsaras, and J. D. Nickels, Description of hydration water in protein (green fluorescent protein) solution, J. Am. Chem. Soc. **139**, 1098 (2017).

[92] M. Lüscher-mattli and M. Rüegg, Thermodynamic functions of biopolymer hydration. II. Enthalpy-entropy compensation in hydrophilic hydration processes, Biopolymers **21**, 419 (1982).

[93] M. Schauperl, M. Podewitz, T. S. Ortner, F. Waibl, A. Thoeny, T. Loerting, and K. R. Liedl, Balance between hydration enthalpy and entropy is important for ice binding surfaces in antifreeze proteins, Sci. Rep. **7**, 11901 (2017).

[94] H. Kiani and D.-W. Sun, Water crystallization and its importance to freezing of foods: A review, Trends Food Sci. Technol. **22**, 407 (2011).

[95] M. P. M. Marques, A. L. M. B. de Carvalho, C. B. Martins, J. D. Silva, M. Sarter, V. García Sakai, J. R. Stewart, and L. A. E. B. de Carvalho, Cellular dynamics as a marker of normal-to-cancer transition in human cells, Sci. Rep. **13**, 21079 (2023).

[96] M. P. M. Marques, I. P. Santos, A. L. M. Batista de Carvalho, A. P. Mamede, C. B. Martins, P. Figueiredo, M. Sarter, V. G. Sakai, and L. A. E. Batista de Carvalho, Water dynamics in human cancer and non-cancer tissues, Phys. Chem. Chem. Phys. **24**, 15406 (2022).

[97] A. Arsiccio and R. Pisano, The ice-water interface and protein stability: A review, J. Pharm. Sci. **109**, 2116 (2020).

[98] https://doi.org/10.5286/ISIS.E.95670743.